Research Article | Vol. 27, No. 5 | 4 Mar 2019 | OPTICS EXPRESS 7196
Optics EXPRESS

Design of anapole mode electromagnetic field enhancement structures for biosensing applications

LAAYA SABRI,[1] QINGLAN HUANG,[2] JUI-NUNG LIU,[2] AND BRIAN T. CUNNINGHAM[2,3,*]

[1]*Department of Electrical Engineering, Tarbiat Modares University, Tehran, Iran*
[2]*Department of Electrical and Computer Engineering, University of Illinois at Urbana-Champaign, Champaign, IL 61800, USA*
[3]*Department of Bioengineering, University of Illinois at Urbana-Champaign, Champaign, IL 61800, USA*
**bcunning@illinois.edu*

Abstract: The design of an all-dielectric nanoantenna based on nonradiating "anapole" modes is studied for biosensing applications in an aqueous environment, using FDTD electromagnetic simulation. The strictly confined electromagnetic field within a circular or rectangular opening at the center of a cylindrical silicon disk produces a single point electromagnetic hotspot with up to 6.5x enhancement of |E|, for the 630-650 nm wavelength range, and we can increase the value up to 25x by coupling additional electromagnetic energy from an underlying PEC-backed substrate. We characterize the effects of the substrate design and slot dimensions on the field enhancement magnitude, for devices operating in a water medium.

© 2019 Optical Society of America under the terms of the OSA Open Access Publishing Agreement

1. Introduction

Although typical surface-based fluorescence assays for detection of protein or nucleic acid molecules for applications that include disease diagnostics [1], genome sequencing [2,3], and pathogen sensing [4] are performed upon glass or plastic surfaces, a variety of nanostructured optical surfaces have demonstrated the ability to increase detected photon output through the mechanisms of enhanced excitation, directional emission and reduced fluorescence lifetimes [5–9]. Such structures include plasmonic gratings, nanoantennas, and photonic crystals (PC) [10–13], which are each capable of efficiently coupling incident light from a laser into surface-confined resonant electric fields (enhanced excitation). PCs have been shown to be especially advantageous because their periodic dielectric structures are comprised of materials without loss at the critical wavelengths, and thus provide moderately high quality factor (Q-factor) resonances that generate strongly confined electric fields near the PC surface. We have shown that PC-enhanced excitation provides >100x improvements in measured detection limits for fluorescent emitters [14].

The use of optically resonant metallic nanostructures to control and concentrate light at sub-diffraction limit scales is currently a well-established capability [15,16]. Surface plasmons, generated by the collective oscillation of conduction electrons near the surface of a metal [17,18], have been the subject of enormous interest for biological sensing applications where a host of nanoparticle shapes, surface structures, and materials [19,20] have been applied for coupling electromagnetic energy into molecules for purposes of label-free biosensing [21], fluorescence enhancement [22–24], and surface-enhanced Raman scattering (SERS) [25,26]. Plasmonic metal nanoantennas' ability to drastically enhance the interaction between a single quantum emitter and its surrounding photonic environment is not only capable of luminescence enhancement, but also ultrafast emission in the picosecond range [27,28] and directional emission control [29,30] – making them nearly ideally suited for

#355300 https://doi.org/10.1364/OE.27.007196
Journal © 2019 Received 13 Dec 2018; revised 12 Feb 2019; accepted 18 Feb 2019; published 27 Feb 2019

Optics EXPRESS

ultrasensitive biodetection of single molecules. However, energy transfer to the free electrons in the metal generates losses, which not only quench fluorescence emission, but also cause substantial Joule heating of the antenna and its environment [31] with sufficient magnitude to melt nanoparticles [32] and to kill cells [33,34]. Thus, plasmonic nanoantennas face fundamental limitations for applications that require moderate temperatures [35] (such as biosensing of proteins, nucleic acids, and small molecules) and high excitation powers [36] desired for fluorescence excitation.

Nanoantennas capture illumination from a source in the far field and compress its optical energy into volumes smaller than the diffraction limit [37–39]. The strong local electromagnetic field enhancements (called "hotspots") enable a wide range of useful applications, such as SERS [40], surface-enhanced infrared absorption (SEIRA) [41–45], spontaneous emission enhancement [46], photothermal biosensing [47], nonlinear nanophotonics [48,49], and nanolasing [50,51]. To achieve large enhancement of the hotspot localized power, which scales with the square of the magnitude of the electric field $|E|^2$, a wide variety of approaches have been reported, including manipulation of the antenna's physical dimensions and materials to tune the resonant wavelength [44,52], using low-loss materials [53,54], impedance matching the input excitation to the nanoantenna [55], and engineering Fano resonances [43,56,57]. To achieve the smallest hotspot volumes and the largest field enhancement factors, plasmonic metal dimer structures have been the most widely studied approach, in which reduced gap size between adjacent metal nanostructures generates the greatest amplification factor [58,59]. When entering the sub-nanometer gap regime, however, it has recently been recently shown that quantum mechanical effects such as nonlocality and electron tunneling stop the hotspot intensity from further increasing monotonically [60–62], and the regime in which biological molecules such as proteins or nucleic acids, no longer fit into the hotspot volume. Thus, to further boost hotspot intensity within a nanoantenna, using designs that do not induce heating of biomolecules, new strategies are needed.

Recently, dielectric nanoantennas comprised of spheres, cylinders, or nanogap dimers of Si, Ge, TiO2, and GaP have been demonstrated as effective alternatives to plasmonic metal antennas [35,63–65]. While the selected materials have little or no loss in the visible or near IR wavelength bands, the dielectric nanoantenna structures support spectral (Mie) resonances that can enhance local near-field electromagnetic intensity [66,67]. Importantly, the dielectric nanoantennas operate through a fundamentally different physical phenomenon from dielectric microresonators (such as PCs or whispering gallery mode structures) that use high quality (Q)-factors to generate field enhancement. Dielectric nanoantennas use small modal volumes with low Q-factors, which provide a broad spectral range for coupling [68]. Furthermore, while metal nanoparticles feature only electric field resonant modes, dielectric nanoantennas have both electric and magnetic modes with similar magnitudes [69–71], and thus offer novel opportunities to engineer the light scattering, radiative decay constants of emitters [35,72], control of directional light emission [73,74], and enhancement of the Raman scattering process. Recent theoretical treatments [75] and experimental demonstrations of Si and GaP dielectric nanoantennas clearly prove their capabilities for low heat conversion [63,64], fluorescence lifetime reduction [35], fluorophore emission enhancement (up to 3600x) [35,65], and SERS enhancement [64].

Our recent work that experimentally demonstrates hybrid coupling between PC moderate Q-factor "micro" cavities and nanoantennas on a PC surface opens opportunities to increase available electromagnetic enhancement factors by additional orders of magnitude, while providing imaging detection instrumentation methods that are capable of measuring the output of many nanoantennas in parallel. Integrating nanoantennas with complementary photonic building blocks, such as evanescent diffraction orders [44,76,77], plasmonic crystals [54], photonic crystals [78] and Fabry–Pérot (FP) cavities [45,79,80] can combine the advantages of both deep-subwavelength field localization and extended storage of

Optics EXPRESS

electromagnetic energy. The nanoantenna-cavity hybrid approach has been shown [81] to boost hotspot intensity up to one order of magnitude, compared to excitation of a solitary nanoantenna that is simply illuminated with a laser in the far field, and therefore can generate more efficient light-matter interactions. Thus, we consider the integration of anapole mode resonators with an external structure to obtain field enhancements greater than achievable with an anapole nanoantenna alone.

Anapoles represent a class of antenna structures that support electric and toroidal dipole moments that result in destructive interference of radiation fields, which is observable in the far field as a pronounced dip in the scattered spectrum at a specific wavelength [82]. While anapoles have been the subject of intense research interest and have been studied using structures that operate in the microwave spectrum [83], recently anapole nanoantennas have been reported at optical frequencies [84] using silicon nanodisks fabricated upon quartz substrates [85].

For a full explanation of anapole nanoantenna physics at optical frequencies, the reader is referred to [85,86]. Briefly, an anapole mode occurs when an electric dipole and a toroidal dipole can be accommodated in the same structure, so that the respective radiation patterns of the electric and toroidal dipole modes can destructively interfere, leading to total scattering cancellation in the far field, with non-zero near-field excitation. For biosensing applications, anapole dielectric nanoantennas are interesting for several reasons: 1. The anapole mode generates a highly concentrated electromagnetic near-field in the center of the structure, 2. The electric fields associated with the mode are confined within the nanoantenna itself, without extending strongly into the surrounding media or to neighboring nanoantennas. 3. The structure is simple to fabricate using well-characterized materials. 4. The anapole wavelength is easily measured by observing the far field scattered spectrum of white light from each individual structure. 5. The anapole mode can be easily excited by external plane wave illumination. 6. As an all-dielectric structure, anapole nanoantennas will not suffer the effects of optical loss and heating that are common to all metal-based plasmonic structures.

To our knowledge, anapole dielectric nanoantenna structures have not been previously considered for biosensing applications. To enable the structure to serve effectively for biodetection, we propose a modification to the silicon nanodisk described in [85] to incorporate a nanohole or nanoslot opening at the disk center [87,88], to coincide with the location of the electric field node of the anapole mode. The hole is a small perturbation to the overall structure, representing a precisely-defined location where light-biomaterial interaction can occur for exciting fluorescent reporters. Further, by fabricating the anapole mode resonator over a dielectric thin film of defined thickness on top of a metal back-reflector, we may take advantage of the hybrid coupling effect to achieve even greater field enhancements. Here, we consider the design of an anapole mode nanoantenna in the context of enhancing localized electromagnetic field intensity for the purpose of enhanced excitation of photon emitters. Our analysis does not consider independent enhancement mechanisms that may also occur due to the Purcell effect or due to enhanced collection efficiency into light collection optics, whose effects are known to multiply with enhanced excitation [89,90].

2. Device structure

While anapole mode structures have been described in a variety of configurations [91–94], here we focus specifically on the design, optimization, and achievable field enhancement performance for biosensing applications, where the device surface would be covered in aqueous media, and the enhanced fields are used to excite fluorescent dye molecules attached to biomolecules (such as nucleic acids or proteins), with excitation wavelengths in the visible spectrum. We also choose materials that are readily available for manufacturable microfabrication and dimensions that are within the capabilities of lithography approaches used in silicon integrated circuit manufacturing. Thus, we anticipate a structure that could be produced uniformly with reproducibility in a conventional integrated circuit foundry.

Optics EXPRESS

The device structure, shown in Fig. 1, is a cylindrical silicon disk (diameter d, height h) with a central opening comprised of either a circular hole (diameter l) or a rectangular slot (length l, width w) on top of a glass substrate, and covered by water. Optionally, the silicon cylinder can be fabricated on a glass (SiO_2) thin film (thickness t) over a metallic back-reflector film comprised of gold, or a theoretically-defined perfect electrical conductor (PEC).

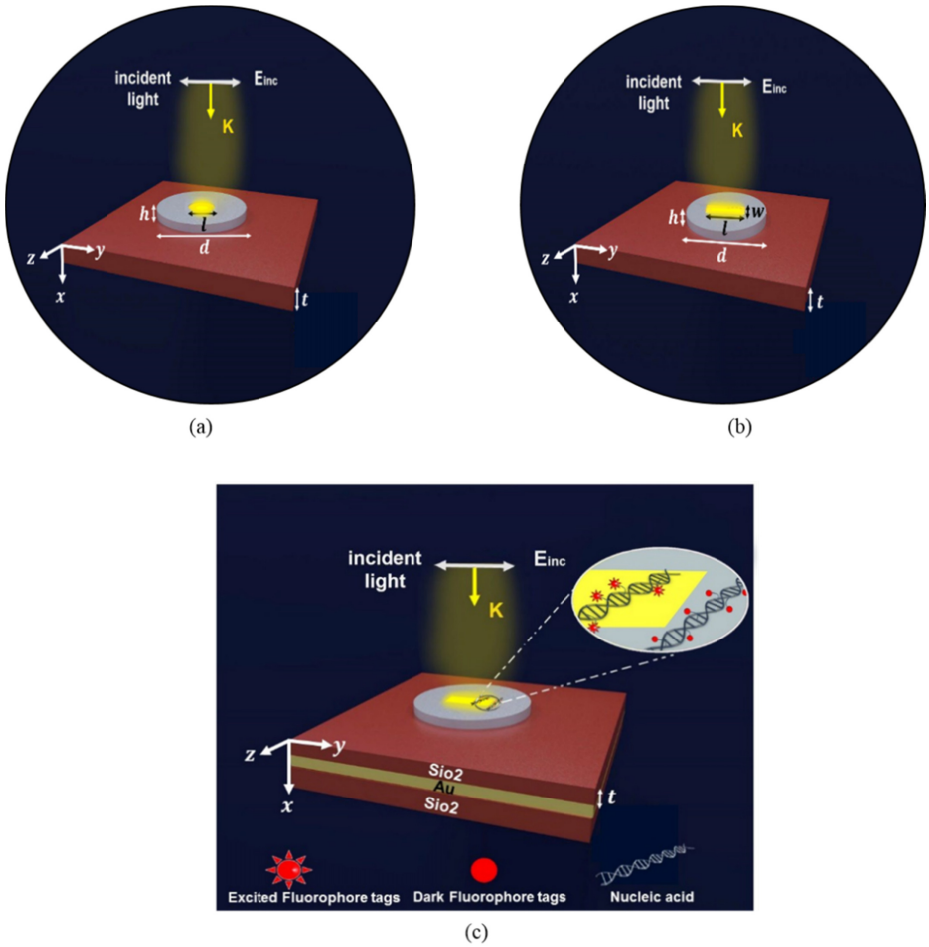

Fig. 1. (a) Schematic diagram of the anapole mode nanoantenna, comprised of a silicon disk with a circular hole provided in the center location in which maximum electric field magnitude occurs fabricated upon a glass substrate, (b) extension of the circular hole to form a rectangular slot, and (c) Anapole mode nanoantenna with a slot provided in the center on a mirror backed dielectric thin film of SiO_2, fabricated upon a glass substrate.

3. Simulation parameters

The Finite Difference Time Domain (FDTD) technique was used for electromagnetic simulation of the device using a commercially available software package (Lumerical). Fixed refractive index values for water (n = 1.33) and SiO_2 (n = 1.4565) were used, while the wavelength-dependent real and imaginary values for the dielectric constants for Si and Au were utilized from Palik and Johnson-Christy respectively [95,96], with values defined in the software package. The silicon disk has a diameter of d = 310nm and a height of h = 50nm. A z-polarized total-field scattered-field (TFSF) source along the x-direction and at the wavelength range of λ = 500-700nm illuminates the structure inside a perfect match layer (PML) boundary conditions. The disk enhancement of the electric field magnitude in the slot

Optics EXPRESS

is calculated, compared to the illuminating electric field intensity of E_0 = 1 V/m. The scattering cross section is defined as $\sigma_{sc} = (1/I_0)\iint (n.S_{sc})ds$ and its local minimum is used as a criterion for determining the resonance frequency of the anapole mode. The integral is taken over the closed surface of the disk in which n shows the normal vector pointing outwards from the surface, S_{sc} is the scattered poynting vector, and I_0 is the incident intensity. It is realized by using six monitors encompassing the TFSF source in the software package. The 100nm thickness of the Au layer was selected to be greater than the skin depth to ensure total reflectivity.

4. Results

Figure 2 shows the scattering cross section and the electric field distribution inside the baseline anapole mode structure covered with water media. The confined electric field at the center of the disk shows the capability of the structure for efficient electromagnetic energy coupling when an opening is incorporated into the center.

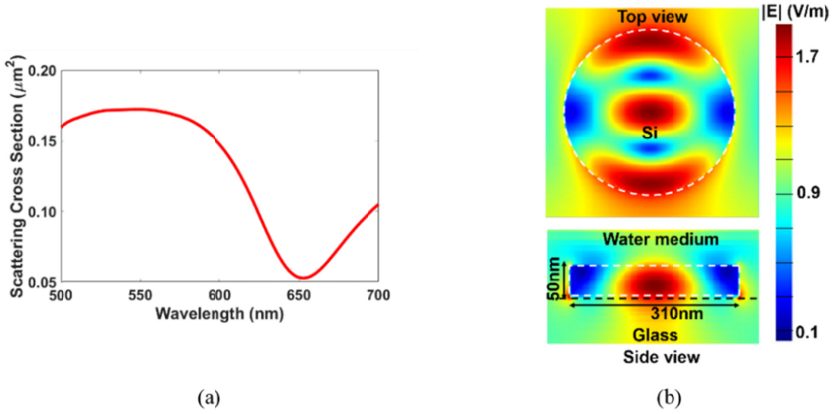

Fig. 2. (a) Scattering cross section of the solid silicon disk on a glass substrate surrounded by water as a function of incident wavelength for an incident plane wave illumination from the top, (b) electric field distribution at the surface and cross section through the center of the disk (Top view and Side view)

The effect of a nanoscale hole opening on field enhancement is shown in Fig. 3. Considering the diameter of protein or nucleic acid biomolecules, the hole diameter is explored in a range of 2.5 - 20nm. The hole diameter has only a small effect upon the resonance wavelength, although its size can be adjusted to maximize electric field enhancement.

Optics EXPRESS

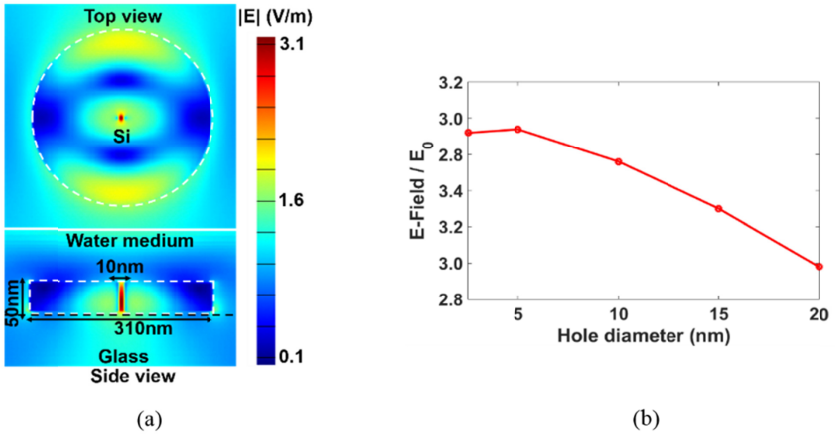

Fig. 3. (a) Electric field distribution at the surface and cross section through the center of a hole-inside disk which is placed on a glass substrate and surrounded by water for the hole diameter of 10nm and an incident plane wave illumination from the top (Top view and side view), (b) maximum enhancement factor inside the hole versus the hole diameter.

Hole elongation in the *y*-direction will cut more current paths and can further increase the enhancement factor, but at the expense of enlarging the cavity volume. The effect of elongating the slot upon the scattered spectrum and the enhancement factor is shown in Fig. 4 by converting the circular hole into a rounded rectangular slot.

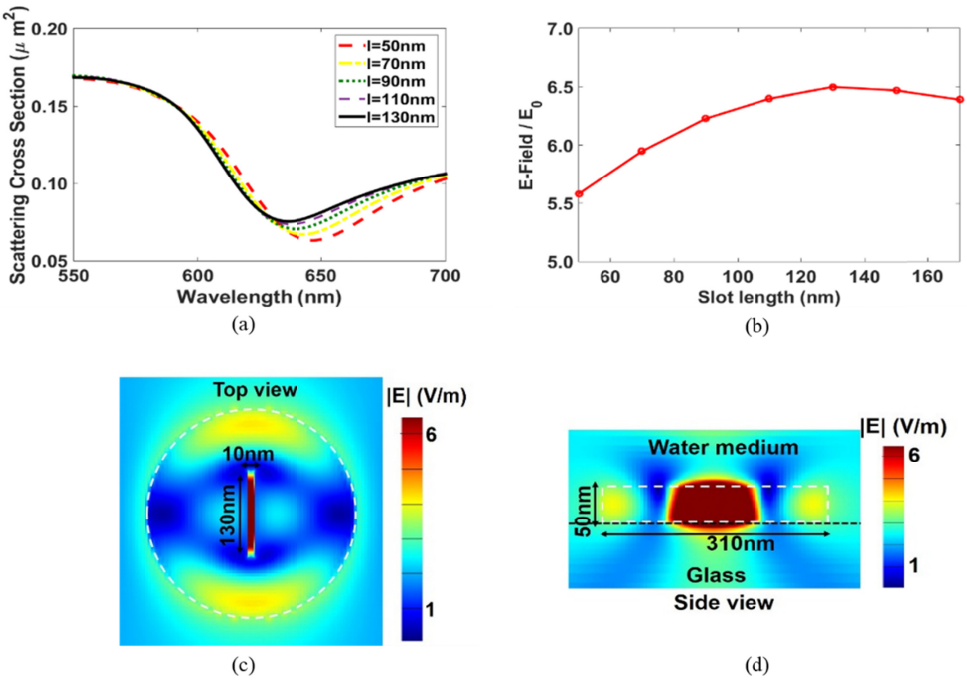

Fig. 4. (a) Scattering cross section, and (b) maximum enhancement factor variation for different slot lengths at the fixed slot width of 10nm for the slotted disk on a glass substrate and surrounded by water under an incident plane wave illumination from the top, electric field distribution at the (c) surface, and (d) cross section for the optimized slot length of 130nm.

When fixing the slot width to 10nm, variation of the slot length shifts the resonance wavelength and changes the enhancement factor. The electric field distribution for the

Optics EXPRESS

optimized value of the slot length is also shown at the surface and cross section of the disk. The slot length that produces the greatest |E| enhancement occurs when the slot fits between the electric field minima. While a slotted disk structure has been investigated previously for field enhancement [88], the modeled structure was a disk suspended in free space, which does not consider the effects of the anapole's interaction with higher refractive index surroundings that include a substrate support and liquid media, which have the effect of reducing the maximally achievable field enhancement. Figure 5 shows the effect of the media refractive index on resonant wavelength and field enhancement, where a 1.3x reduction in field enhancement occurs when substituting air for water on top of the device. The electric field will no longer remain confined inside the disk by increasing the refractive indices of the medium, resulting in the Q-factor and the electric field becoming smaller when the index of the surrounding medium increases.

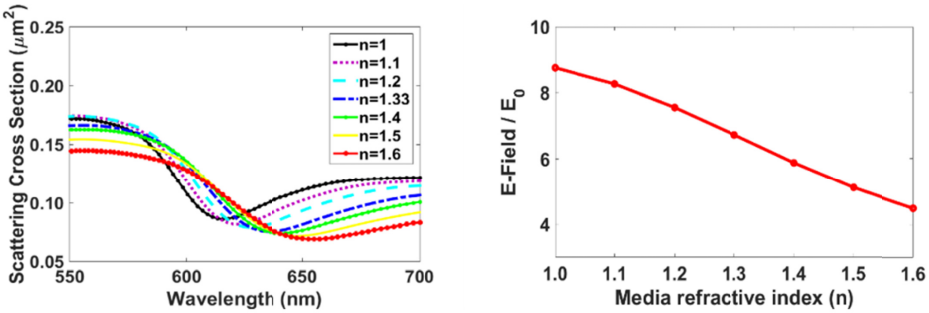

Fig. 5. (a) Scattering cross section, and (b) maximum enhancement factor variation of the slotted disk on a glass substrate and surrounded by the environments with different refractive indices.

An efficient substrate design can significantly rectify the field reduction, by using a hybrid strategy to increase the energy coupling to the anapole mode structure. Hybrid resonator systems have been utilized effectively in previous research. For example, in a hybrid system consisting of a silicon nanoparticle and metallic film [97], the near-field enhancement is ascribed to the interaction of the electric and magnetic dipole resonance modes of the dielectric nanoparticle with the metal film. The hybrid resonance in a dielectric-metal resonator reported in [98] has been utilized effectively to squeeze the field inside the structure. The field enhancement of the aforesaid hybrid structures is achieved at the interface of the nanoparticle and the metal film, which is required for a precisely sized molecular spacer layer. Periodic arrays of dielectric nanoparticles on dielectric-based substrates have also been demonstrated for field enhancement [99,100].

An effective substrate design can be made by considering the constitutive modes of the anapole mode and employing a method for affecting these modes. The radiation of the electric dipole (ED) and toroidal dipole (TD), which are the two components of the anapole mode, is drastically altered when they get close to the surface of a simple electric mirror that can change the scattering level and energy coupling to the structure. The 2x enhancement of the electric field at a quarter wavelength distance of the mirror is simply a consequence of constructive interference between the incident and reflected waves, which increases the stored energy at the plane of the anapole mode.

Furthermore, it can be shown that by decreasing the layer thickness beyond a quarter wavelength, a greater Q-factor can be achieved for the hybrid system, which in turn is capable of further enhancing the electromagnetic field in the anapole structure. This high Q-factor is obtained under the conditions for which scattering is minimized and the anapole mode's electromagnetic field does not intersect with the metal of the underlying mirror. At shorter wavelengths, the higher resonance frequency and the scattering cancelation of the ED and TD

Optics EXPRESS

modes adjacent to the mirror keeps the Q-factor at a high level, whereas the mode distortion inside the disk reduces the storage energy and prevents further field enhancement. The enhanced Q-factor of the anapole mode on a mirror-backed substrate in comparison to the poor Q-factor of the single silicon disk is responsible for the greater enhancement of the electric field magnitude. The required thickness for obtaining the highest Q-factor can be easily achieved by coating the metal with a layer of low index dielectric material.

The mirror-backed slotted disk is illustrated in Fig. 1(c). A layer of SiO_2 between the disk and mirror provides the 180 degree phase shift of the electric field upon reflection from the mirror to reach a phase coherency in the slot position. The SiO_2 thickness can be adjusted for achieving the optimized field enhancement through the Q-factor increment. We develop the concept by using the perfect electric conductor (PEC) as the underlying metal, and subsequently can model the effects using the dielectric parameters of gold.

The wavelength and field enhancement variation obtained by changing the SiO_2 layer thickness is shown in Fig. 6.

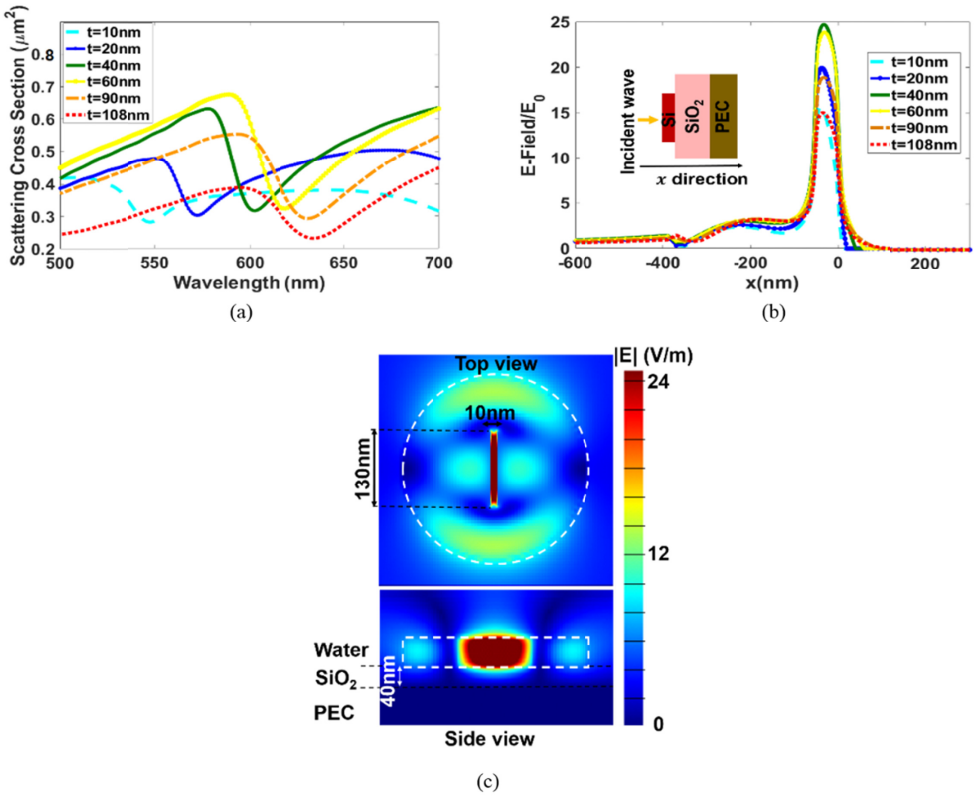

Fig. 6. (a) Scattering cross section, and (b) field distribution along the *x*-direction going up through the center of the slotted disk on a PEC mirror for different thickness of the SiO_2 layer and under incident plane wave illumination from the top side, (c) top and cross section view of the electric field distribution inside the slotted disk at the optimized SiO_2 layer thickness of 40nm.

The resonance wavelength of the anapole mode is shifted by the metal, and it returns to its initial value by increasing the SiO_2 layer thickness. Scattering reduction at the lower thickness of the SiO_2 layer is ascribed to the scattering cancelation of the anapole mode at these thicknesses. As expected, 2x magnification of |E| occurs when the SiO_2 is $\lambda/4$ of the illumination wavelength due to the phase compensation. The greater enhanced field at the thickness of 40nm is due to the higher Q-factor which is obtained at this thickness. The total

Optics EXPRESS

stored energy inside the disk (calculated by Comsol software package) and the Q-factor as a function of SiO_2 layer thickness is shown in Fig. 7. The highest value for stored energy occurs for a SiO_2 thickness of 40nm. However, 20nm SiO_2 thickness corresponds to the maximum Q-factor due to the higher resonance frequency and lower radiation losses of the slotted disk.

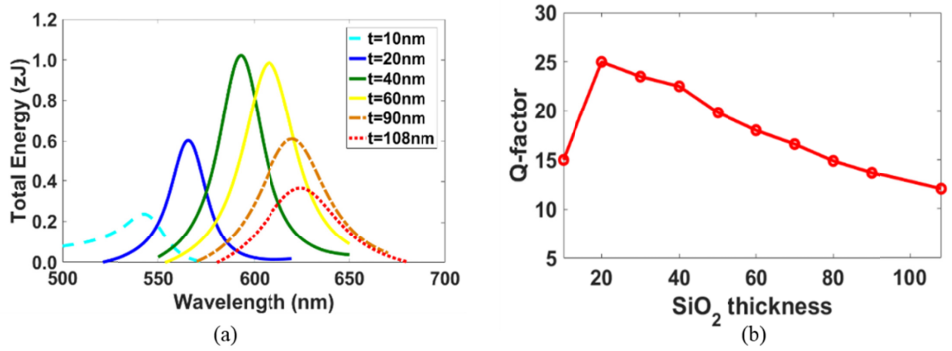

Fig. 7. (a) The total (Electric + Magnetic) stored energy inside and nearby the slotted disk on PEC-backed substrate, (b) the estimated Q-factor of the structure at different SiO_2 thicknesses.

The Q-factor is estimated by fitting a quadratic curve to the energy spectrum [101]. The Q-factors obtained for all thicknesses of SiO_2 gap layer are greater than the Q-factor, Q = 8.5, of the single slotted disk without a substrate. Radiation cancelation of the mode at the lower SiO_2 thicknesses increases the Q-factor; however trying for further scattering cancelation by further reducing the distance between the nanodisk and the mirror distorts the field distribution on the bottom side of the nanodisk, which results in biasing the position of the anapole mode toward the upper side of the disk. We find that the resulting mode distribution reduces the stored energy and, as a consequence, the enhancement factor. The field reduction of the single slotted disk at thinner thicknesses in Fig. 8 provides evidence for this claim. The electric field distortion inside the disk is evident from Fig. 9 for the thinner thicknesses of the SiO_2 layer.

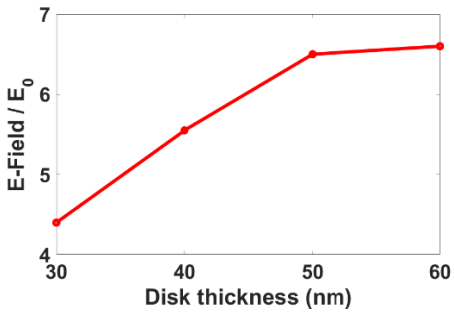

Fig. 8. The maximum enhancement factor at the center of the slotted disk placed on a glass substrate and surrounded by water for different disk thicknesses.

Optics EXPRESS

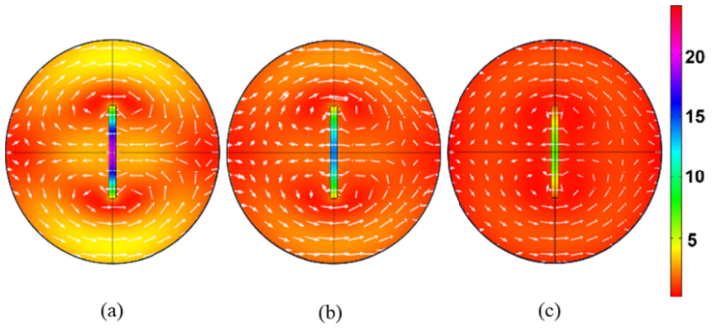

Fig. 9. Electric field distribution at the lower side of the slotted disk placed on a PEC-backed substrate under a plane wave illumination from the top for different SiO_2 thicknesses of (a) 40nm, (b) 20nm, and (c) 10nm. The Figs are from comsol software package to enable the vector and intensity illustration at the same time.

We show that maximum field enhancement of 25x can be achieved for a SiO_2 layer thickness of 40nm, which coincides with the SiO_2 layer that provides the greatest stored energy. Using the PEC for the reflective layer ensures us that the enhancement is not caused by surface plasmon polaritons. The scattering and enhancement property of the structure by replacing the PEC with a 100nm thin layer of Au is shown in Fig. 10, which shows that the maximum field enhancement value is a bit lower than the PEC case, due to the gold's optical loss. Also, the required thickness of SiO_2 for doubled enhancement and critical coupling is 30nm lower than when a PEC layer is considered due to the different phase reference plane between PEC and the gold mirror. The phase reference plane of the PEC is exactly at its surface, while it is located slightly inside the metal for the gold mirror. The penetration depth (δ) of the gold at a defined wavelength specifies the location of the phase reference plane. At the operating wavelength of our designed structure, δ is calculated as 30nm, which is equal to the difference between the optimal SiO_2 thickness between the PEC and gold mirror. Figure 11 shows the validity of this claim. The electric field distribution inside the SiO_2 layer on top of the PEC and gold mirror reaches its maximum at the thickness value difference of approximately 30nm.

Optics EXPRESS

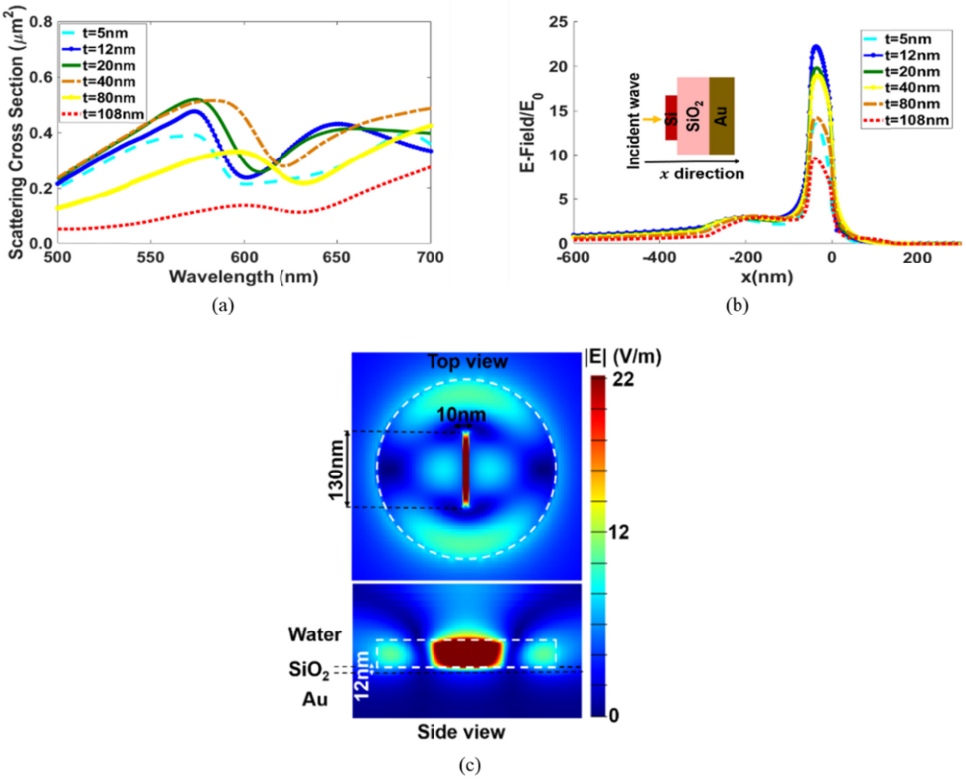

Fig. 10. (a) Scattering cross section, and (b) field distribution along the *x*-direction going up through the center of the slotted disk on a gold mirror for different thickness of the SiO_2 layer and under incident plane wave illumination from the top side, (c) top and cross section view of the electric field distribution inside the slotted disk at the optimized SiO_2 layer thickness of 12nm.

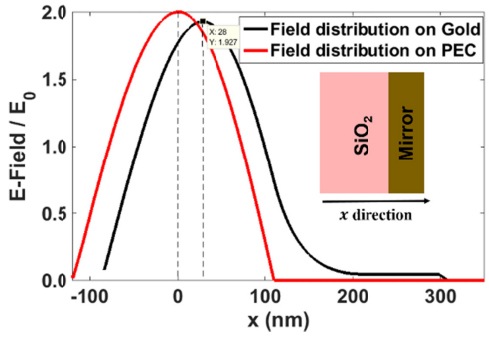

Fig. 11. Electric field linear distribution along the SiO_2 layer on top of the PEC and gold mirrors.

5. Discussion

We consider the utilization of the anapole mode nanoantenna structure in the context of exciting fluorescent emitters used to label nucleic acid and protein biomolecular interactions. The opening in the center of the anapole mode disk structure is designed to be approximately the same size as a single biomolecule, so that one molecule located within the hole will experience greater excitation intensity than any molecule in the surrounding liquid media or attached to any location outside the hole. Thus, when the entire surface that contains the

Optics EXPRESS

structure is illuminated with a normal-incidence plane wave with a magnitude of 1 V/m, an emitter inside the electromagnetic hotspot will emit photons with a scaling factor that multiplies with the power associated with the electromagnetic field. Thus, fluorophore excitation enhancement will scale with the square of the electric field magnitude enhancements predicted in Fig. 10 generating up to 480 gains. Further gains in hotspot-associated emission intensity may also be achieved through the mechanism of Purcell enhancement, in which the fluorescent lifetime of emitters is reduced when they are located within an optical resonator [88]. Through this mechanism, a single fluorescent emitter may be "recycled" more quickly through its transition from the excited state to the ground state, and thus more photons/fluorophore are observed in the far field. Finally, emitted photons originating from the center of the anapole mode will be directed outward by the dispersion of the nanoantenna, providing an opportunity for a further "enhanced extraction" effect. Due to the presence of the underlying mirror, emitted photons in the downward direction will have the opportunity to back-reflect to the optics that gather the fluorescent signal (such as a microscope objective). Enhanced extraction effects are a combined function of the spatial distributions of photons originating in the anapole mode center and the numerical aperture of the light collection optics [102], and thus must be considered separately from enhancement of photon excitation due to hotspot electric field intensity.

Because the effects of these enhancement mechanisms are multiplicative, we believe that the structure presented here is promising for enhanced fluorescence single-molecule biosensing applications with very substantial overall enhancement for emitters located within the well-defined hotspot volume, where the volumes shown here range from 0.001 – 0.065 fL. The overall enhancement is calculated using the expression $F_p \times (E/E_0)^2 \times G_{Ex}$, where F_p represents the Purcell factor and G_{Ex} represents the gain from enhanced efficiency of extraction of emitted photons from the hotspot into the numerical aperture of light collection optics positioned above the device. For example [88], reports Purcell enhancements of 550x and 740x at two different wavelengths for a perfect dipole emitter in an anapole structure. For the water-immersed structures reported here, we estimate a potential Purcell factor value of $F_p = 210x$, calculated as the ratio of energy dissipation rates of an electric dipole P/P_0 [103]. This value is derived from the FDTD software package that offers a methodology for estimating Purcell enhancements [92] in which the structure is excited with a y-polarized dipole placed inside the hotspot of the disk. As an initial estimate of the G_{Ex} available from enhanced extraction effects [104], reports a 20-30x enhanced collection of emission from a dipole upon a PEC backed substrate with a 0.1-1 numerical aperture objective. Therefore, the prospects for achieving overall gains for fluorescent emitters within the anapole mode nanoantenna of $F_p \times (E/E_0)^2 \times G_{Ex} = (210) \times (480) \times (25) = 2{,}520{,}000$ would appear to be feasible, and is motivating for experimental realization and testing of the simulated structures reported in this work.

A representative metal-based structure with similar hotspot volume is the subwavelength aperture zero mode waveguides (ZMWs), comprised of a circular hole in an aluminum thin film to provide observation volumes in the zeptoliter range. The small volume of confinement allows for single molecule characterization and further optical application including real-time imaging of protein-protein interactions, real-time observation of enzymatic activity, and single molecule DNA sequencing [105–109], but does not offer the opportunity for resonant field enhancement, except by some considerations [110,111].

We envision applications for the structure in which an array of anapole mode nanoantennas may be prepared with individual capturing molecules located within each central hole, and illuminated by an external excitation source while biomolecules in the liquid media bind/unbind to the molecules in the hotspots. Due to the enhancements afforded to fluorophores captured within the hotspot, biomolecular events occurring there may be

observed with high signal-to-noise, representing the emissions from single fluorophores associated with single molecules. Observation of the rates of biomolecule capture/release and fluorophore emission wavelength will enable measurement of single biomolecule binding dynamics and processes that include conformation change and association/dissociation. It is also possible to envision structures in which a pore is included inside the substrate of the anapole mode nanoantenna, exactly beneath of its embedded hole, so that molecules may be rapidly excited while they flow through the structure.

Funding

National Science Foundation (CBET 1512043).

References

1. K. S. Park, R. C. Charles, E. T. Ryan, R. Weissleder, and H. Lee, "Fluorescence Polarization Based Nucleic Acid Testing for Rapid and Cost-Effective Diagnosis of Infectious Disease," Chemistry **21**(46), 16359–16363 (2015).
2. J. M. Prober, G. L. Trainor, R. J. Dam, F. W. Hobbs, C. W. Robertson, R. J. Zagursky, A. J. Cocuzza, M. A. Jensen, and K. Baumeister, "A system for rapid DNA sequencing with fluorescent chain-terminating dideoxynucleotides," Science **238**(4825), 336–341 (1987).
3. J. H. Lee, E. R. Daugharthy, J. Scheiman, R. Kalhor, T. C. Ferrante, R. Terry, B. M. Turczyk, J. L. Yang, H. S. Lee, J. Aach, K. Zhang, and G. M. Church, "Fluorescent in situ sequencing (FISSEQ) of RNA for gene expression profiling in intact cells and tissues," Nat. Protoc. **10**(3), 442–458 (2015).
4. N. C. Cady, S. Stelick, M. V. Kunnavakkam, and C. A. Batt, "Real-time PCR detection of Listeria monocytogenes using an integrated microfluidics platform," Sensor. Actuat. B-Chem. **107**(1), 332–341 (2005).
5. J. R. Lakowicz, "Radiative decay engineering: biophysical and biomedical applications," Anal. Biochem. **298**(1), 1–24 (2001).
6. S. Fan and J. D. Joannopoulos, "Analysis of guided resonances in photonic crystal slabs," Phys. Rev. B Condens. Matter Mater. Phys. **65**(23), 235112 (2002).
7. K. A. Willets and R. P. Van Duyne, "Localized surface plasmon resonance spectroscopy and sensing," Annu. Rev. Phys. Chem. **58**(1), 267–297 (2007).
8. P. Anger, P. Bharadwaj, and L. Novotny, "Enhancement and quenching of single-molecule fluorescence," Phys. Rev. Lett. **96**(11), 113002 (2006).
9. H. Hori, K. Tawa, K. Kintaka, J. Nishii, and Y. Tatsu, "Influence of groove depth and surface profile on fluorescence enhancement by grating-coupled surface plasmon resonance," Opt. Rev. **16**(2), 216–221 (2009).
10. E. L. Moal, E. Fort, S. Lévêque-Fort, F. P. Cordelières, M.-P. Fontaine-Aupart, and C. Ricolleau, "Enhanced fluorescence cell imaging with metal-coated slides," Biophys. J. **92**(6), 2150–2161 (2007).
11. L. C. Estrada, O. E. Martinez, M. Brunstein, S. Bouchoule, L. Le-Gratiet, A. Talneau, I. Sagnes, P. Monnier, J. A. Levenson, and A. M. Yacomotti, "Small volume excitation and enhancement of dye fluorescence on a 2D photonic crystal surface," Opt. Express **18**(4), 3693–3699 (2010).
12. A. Kinkhabwala, Z. Yu, S. Fan, Y. Avlasevich, K. Müllen, and W. E. Moerner, "Large single-molecule fluorescence enhancements produced by a bowtie nanoantenna," Nat. Photonics **3**(11), 654–657 (2009).
13. K. Tawa, H. Hori, K. Kintaka, K. Kiyosue, Y. Tatsu, and J. Nishii, "Optical microscopic observation of fluorescence enhanced by grating-coupled surface plasmon resonance," Opt. Express **16**(13), 9781–9790 (2008).
14. A. Pokhriyal, M. Lu, V. Chaudhery, C.-S. Huang, S. Schulz, and B. T. Cunningham, "Photonic crystal enhanced fluorescence using a quartz substrate to reduce limits of detection," Opt. Express **18**(24), 24793–24808 (2010).
15. J. A. Schuller, E. S. Barnard, W. Cai, Y. C. Jun, J. S. White, and M. L. Brongersma, "Plasmonics for extreme light concentration and manipulation," Nat. Mater. **9**(3), 193–204 (2010).
16. M. I. Stockman, "Nanoplasmonics: past, present, and glimpse into future," Opt. Express **19**(22), 22029–22106 (2011).
17. S. A. Maier, *Plasmonics - Fundamentals and Applications* (Springer, 2007).
18. M. I. Stockman, "Nanoplasmonics: The physics behind the applications," Phys. Today **64**(2), 39–44 (2011).
19. S. A. Maier and H. A. Atwater, "Plasmonics: Localization and guiding of electromagnetic energy in metal/dielectric structures," J. Appl. Phys. **98**(1), 10 (2005).
20. L. Novotny and N. van Hulst, "Antennas for light," Nat. Photonics **5**(2), 83–90 (2011).
21. J. N. Anker, W. P. Hall, O. Lyandres, N. C. Shah, J. Zhao, and R. P. Van Duyne, "Biosensing with plasmonic nanosensors," Nat. Mater. **7**(6), 442–453 (2008).
22. J. Enderlein, "Theoretical study of single molecule fluorescence in a metallic nanocavity," Appl. Phys. Lett. **80**(2), 315–317 (2002).
23. J. R. Lakowicz, "Plasmonics in biology and plasmon-controlled fluorescence," Plasmonics **1**(1), 5–33 (2006).
24. Y. Liu and S. Blair, "Fluorescence enhancement from an array of subwavelength metal apertures," Opt. Lett. **28**(7), 507–509 (2003).
25. S.-M. Kim, W. Zhang, and B. T. Cunningham, "Coupling discrete metal nanoparticles to photonic crystal surface resonant modes and application to Raman spectroscopy," Opt. Express **18**(5), 4300–4309 (2010).

Optics EXPRESS

26. S. M. Kim, W. Zhang, and B. T. Cunningham, "Photonic crystals with SiO(2)-Ag "post-cap" nanostructure coatings for surface enhanced Raman spectroscopy," Appl. Phys. Lett. **93**(14), 143112 (2008).
27. G. M. Akselrod, C. Argyropoulos, T. B. Hoang, C. Ciraci, C. Fang, J. N. Huang, D. R. Smith, and M. H. Mikkelsen, "Probing the mechanisms of large Purcell enhancement in plasmonic nanoantennas," Nat. Photonics **8**(11), 835–840 (2014).
28. T. B. Hoang, G. M. Akselrod, C. Argyropoulos, J. Huang, D. R. Smith, and M. H. Mikkelsen, "Ultrafast spontaneous emission source using plasmonic nanoantennas," Nat. Commun. **6**(1), 7788 (2015).
29. A. G. Curto, G. Volpe, T. H. Taminiau, M. P. Kreuzer, R. Quidant, and N. F. van Hulst, "Unidirectional emission of a quantum dot coupled to a nanoantenna," Science **329**(5994), 930–933 (2010).
30. Y. C. Jun, K. C. Y. Huang, and M. L. Brongersma, "Plasmonic beaming and active control over fluorescent emission," Nat. Commun. **2**(1), 283 (2011).
31. G. Baffou, R. Quidant, and C. Girard, "Heat generation in plasmonic nanostructures: Influence of morphology," Appl. Phys. Lett. **94**(15), 153109 (2009).
32. A. O. Govorov, W. Zhang, T. Skeini, H. Richardson, J. Lee, and N. A. Kotov, "Gold nanoparticle ensembles as heaters and actuators: melting and collective plasmon resonances," Nanoscale Res. Lett. **1**(1), 84–90 (2006).
33. D. Lapotko, "Therapy with gold nanoparticles and lasers: what really kills the cells?" Nanomedicine (Lond.) **4**(3), 253–256 (2009).
34. E. Y. Hleb, J. H. Hafner, J. N. Myers, E. Y. Hanna, B. C. Rostro, S. A. Zhdanok, and D. O. Lapotko, "LANTCET: elimination of solid tumor cells with photothermal bubbles generated around clusters of gold nanoparticles," Nanomedicine (Lond.) **3**(5), 647–667 (2008).
35. J. Cambiasso, G. Grinblat, Y. Li, A. Rakovich, E. Cortés, and S. A. Maier, "Bridging the Gap between Dielectric Nanophotonics and the Visible Regime with Effectively Lossless Gallium Phosphide Antennas," Nano Lett. **17**(2), 1219–1225 (2017).
36. M. D. King, S. Khadka, G. A. Craig, and M. D. Mason, "Effect of local heating on the SERS efficiency of optically trapped prismatic nanoparticles," J. Phys. Chem. C **112**(31), 11751–11757 (2008).
37. M. Agio and A. Alù, *Optical Antennas* (Cambridge University 2013).
38. L. Novotny and N. van Hulst, "Antennas for light," Nat. Photonics **5**(2), 83–90 (2011).
39. V. Giannini, A. I. Fernández-Domínguez, S. C. Heck, and S. A. Maier, "Plasmonic nanoantennas: fundamentals and their use in controlling the radiative properties of nanoemitters," Chem. Rev. **111**(6), 3888–3912 (2011).
40. K. Kneipp, M. Moskovits, and H. Kneipp, *Surface-Enhanced Raman Scattering Physics and Applications* (Springer, 2006).
41. F. Neubrech, C. Huck, K. Weber, A. Pucci, and H. Giessen, "Surface-Enhanced Infrared Spectroscopy Using Resonant Nanoantennas," Chem. Rev. **117**(7), 5110–5145 (2017).
42. F. Neubrech, A. Pucci, T. W. Cornelius, S. Karim, A. García-Etxarri, and J. Aizpurua, "Resonant plasmonic and vibrational coupling in a tailored nanoantenna for infrared detection," Phys. Rev. Lett. **101**(15), 157403 (2008).
43. C. Wu, A. B. Khanikaev, R. Adato, N. Arju, A. A. Yanik, H. Altug, and G. Shvets, "Fano-resonant asymmetric metamaterials for ultrasensitive spectroscopy and identification of molecular monolayers," Nat. Mater. **11**(1), 69–75 (2011).
44. R. Adato, A. A. Yanik, J. J. Amsden, D. L. Kaplan, F. G. Omenetto, M. K. Hong, S. Erramilli, and H. Altug, "Ultra-sensitive vibrational spectroscopy of protein monolayers with plasmonic nanoantenna arrays," Proc. Natl. Acad. Sci. U.S.A. **106**(46), 19227–19232 (2009).
45. L. V. Brown, X. Yang, K. Zhao, B. Y. Zheng, P. Nordlander, and N. J. Halas, "Fan-shaped gold nanoantennas above reflective substrates for surface-enhanced infrared absorption (SEIRA)," Nano Lett. **15**(2), 1272–1280 (2015).
46. M. Pelton, "Modified spontaneous emission in nanophotonic structures," Nat. Photonics **9**(7), 427–435 (2015).
47. P. Zijlstra, P. M. R. Paulo, and M. Orrit, "Optical detection of single non-absorbing molecules using the surface plasmon resonance of a gold nanorod," Nat. Nanotechnol. **7**(6), 379–382 (2012).
48. M. Kauranen and A. V. Zayats, "Nonlinear plasmonics," Nat. Photonics **6**(11), 737–748 (2012).
49. H. Aouani, M. Rahmani, M. Navarro-Cía, and S. A. Maier, "Third-harmonic-upconversion enhancement from a single semiconductor nanoparticle coupled to a plasmonic antenna," Nat. Nanotechnol. **9**(4), 290–294 (2014).
50. R. F. Oulton, V. J. Sorger, T. Zentgraf, R.-M. Ma, C. Gladden, L. Dai, G. Bartal, and X. Zhang, "Plasmon lasers at deep subwavelength scale," Nature **461**(7264), 629–632 (2009).
51. M. A. Noginov, G. Zhu, A. M. Belgrave, R. Bakker, V. M. Shalaev, E. E. Narimanov, S. Stout, E. Herz, T. Suteewong, and U. Wiesner, "Demonstration of a spaser-based nanolaser," Nature **460**(7259), 1110–1112 (2009).
52. A. Alù and N. Engheta, "Tuning the scattering response of optical nanoantennas with nanocircuit loads," Nat. Photonics **2**(5), 307–310 (2008).
53. G. V. Naik, V. M. Shalaev, and A. Boltasseva, "Alternative plasmonic materials: beyond gold and silver," Adv. Mater. **25**(24), 3264–3294 (2013).
54. Y. Chu, M. G. Banaee, and K. B. Crozier, "Double-resonance plasmon substrates for surface-enhanced Raman scattering with enhancement at excitation and stokes frequencies," ACS Nano **4**(5), 2804–2810 (2010).
55. T. J. Seok, A. Jamshidi, M. Kim, S. Dhuey, A. Lakhani, H. Choo, P. J. Schuck, S. Cabrini, A. M. Schwartzberg, J. Bokor, E. Yablonovitch, and M. C. Wu, "Radiation engineering of optical antennas for maximum field enhancement," Nano Lett. **11**(7), 2606–2610 (2011).

Optics EXPRESS

56. J. A. Fan, C. Wu, K. Bao, J. Bao, R. Bardhan, N. J. Halas, V. N. Manoharan, P. Nordlander, G. Shvets, and F. Capasso, "Self-assembled plasmonic nanoparticle clusters," Science **328**(5982), 1135–1138 (2010).
57. B. Luk'yanchuk, N. I. Zheludev, S. A. Maier, N. J. Halas, P. Nordlander, H. Giessen, and C. T. Chong, "The Fano resonance in plasmonic nanostructures and metamaterials," Nat. Mater. **9**(9), 707–715 (2010).
58. P. J. Schuck, D. P. Fromm, A. Sundaramurthy, G. S. Kino, and W. E. Moerner, "Improving the mismatch between light and nanoscale objects with gold bowtie nanoantennas," Phys. Rev. Lett. **94**(1), 017402 (2005).
59. D.-K. Lim, K.-S. Jeon, H. M. Kim, J.-M. Nam, and Y. D. Suh, "Nanogap-engineerable Raman-active nanodumbbells for single-molecule detection," Nat. Mater. **9**(1), 60–67 (2010).
60. W. Zhu, R. Esteban, A. G. Borisov, J. J. Baumberg, P. Nordlander, H. J. Lezec, J. Aizpurua, and K. B. Crozier, "Quantum mechanical effects in plasmonic structures with subnanometre gaps," Nat. Commun. **7**(1), 11495 (2016).
61. C. Ciracì, R. T. Hill, J. J. Mock, Y. Urzhumov, A. I. Fernández-Domínguez, S. A. Maier, J. B. Pendry, A. Chilkoti, and D. R. Smith, "Probing the ultimate limits of plasmonic enhancement," Science **337**(6098), 1072–1074 (2012).
62. J. Zuloaga, E. Prodan, and P. Nordlander, "Quantum description of the plasmon resonances of a nanoparticle dimer," Nano Lett. **9**(2), 887–891 (2009).
63. P. Albella, R. A. de la Osa, F. Moreno, and S. A. Maier, "Electric and Magnetic Field Enhancement with Ultralow Heat Radiation Dielectric Nanoantennas: Considerations for Surface-Enhanced Spectroscopies," ACS Photonics **1**(6), 524–529 (2014).
64. M. Caldarola, P. Albella, E. Cortés, M. Rahmani, T. Roschuk, G. Grinblat, R. F. Oulton, A. V. Bragas, and S. A. Maier, "Non-plasmonic nanoantennas for surface enhanced spectroscopies with ultra-low heat conversion," Nat. Commun. **6**(1), 7915 (2015).
65. R. Regmi, J. Berthelot, P. M. Winkler, M. Mivelle, J. Proust, F. Bedu, I. Ozerov, T. Begou, J. Lumeau, H. Rigneault, M. F. García-Parajó, S. Bidault, J. Wenger, and N. Bonod, "All-Dielectric Silicon Nanogap Antennas To Enhance the Fluorescence of Single Molecules," Nano Lett. **16**(8), 5143–5151 (2016).
66. M. M. Sigalas, D. A. Fattal, R. S. Williams, S. Y. Wang, and R. G. Beausoleil, "Electric field enhancement between two Si microdisks," Opt. Express **15**(22), 14711–14716 (2007).
67. G. Boudarham, R. Abdeddaim, and N. Bonod, "Enhancing the magnetic field intensity with a dielectric gap antenna," Appl. Phys. Lett. **104**(2), 021117 (2014).
68. A. Devilez, X. Zambrana-Puyalto, B. Stout, and N. Bonod, "Mimicking localized surface plasmons with dielectric particles," Phys. Rev. B Condens. Matter Mater. Phys. **92**(24), 241412 (2015).
69. A. B. Evlyukhin, S. M. Novikov, U. Zywietz, R. L. Eriksen, C. Reinhardt, S. I. Bozhevolnyi, and B. N. Chichkov, "Demonstration of magnetic dipole resonances of dielectric nanospheres in the visible region," Nano Lett. **12**(7), 3749–3755 (2012).
70. A. I. Kuznetsov, A. E. Miroshnichenko, Y. H. Fu, J. Zhang, and B. Luk'yanchuk, "Magnetic light," Sci. Rep. **2**(1), 492 (2012).
71. U. Zywietz, A. B. Evlyukhin, C. Reinhardt, and B. N. Chichkov, "Laser printing of silicon nanoparticles with resonant optical electric and magnetic responses," Nat. Commun. **5**(1), 3402 (2014).
72. B. Rolly, B. Bebey, S. Bidault, B. Stout, and N. Bonod, "Promoting magnetic dipolar transition in trivalent lanthanide ions with lossless Mie resonances," Phys. Rev. B Condens. Matter Mater. Phys. **85**(24), 245432 (2012).
73. N. Bonod, A. Devilez, B. Rolly, S. Bidault, and B. Stout, "Ultracompact and unidirectional metallic antennas," Phys. Rev. B Condens. Matter Mater. Phys. **82**(11), 115429 (2010).
74. A. Devilez, B. Stout, and N. Bonod, "Compact metallo-dielectric optical antenna for ultra directional and enhanced radiative emission," ACS Nano **4**(6), 3390–3396 (2010).
75. A. E. Krasnok, A. E. Miroshnichenko, P. A. Belov, and Y. S. Kivshar, "All-dielectric optical nanoantennas," Opt. Express **20**(18), 20599–20604 (2012).
76. W. Zhou and T. W. Odom, "Tunable subradiant lattice plasmons by out-of-plane dipolar interactions," Nat. Nanotechnol. **6**(7), 423–427 (2011).
77. Y. Chu, E. Schonbrun, T. Yang, and K. B. Crozier, "Experimental observation of narrow surface plasmon resonances in gold nanoparticle arrays," Appl. Phys. Lett. **93**(18), 181108 (2008).
78. M. Fränzl, S. Moras, O. D. Gordan, and D. R. Zahn, "Interaction of One-Dimensional Photonic Crystals and Metal Nanoparticle Arrays and Its Application for Surface-Enhanced Raman Spectroscopy," J. Phys. Chem. C **122**(18), 10153–10158 (2018).
79. M. A. Schmidt, D. Y. Lei, L. Wondraczek, V. Nazabal, and S. A. Maier, "Hybrid nanoparticle-microcavity-based plasmonic nanosensors with improved detection resolution and extended remote-sensing ability," Nat. Commun. **3**(1), 1108 (2012).
80. D. Chanda, K. Shigeta, T. Truong, E. Lui, A. Mihi, M. Schulmerich, P. V. Braun, R. Bhargava, and J. A. Rogers, "Coupling of plasmonic and optical cavity modes in quasi-three-dimensional plasmonic crystals," Nat. Commun. **2**(1), 479 (2011).
81. J.-N. Liu, Q. Huang, K.-K. Liu, S. Singamaneni, and B. T. Cunningham, "Nanoantenna-Microcavity Hybrids with Highly Cooperative Plasmonic-Photonic Coupling," Nano Lett. **17**(12), 7569–7577 (2017).
82. G. N. Afanasiev and Y. P. Stepanovsky, "The Electromagnetic-Field of Elementary Time-Dependent Toroidal Sources," J. Phys. Math. Gen. **28**(16), 4565–4580 (1995).

Optics EXPRESS

83. V. A. Fedotov, A. V. Rogacheva, V. Savinov, D. P. Tsai, and N. I. Zheludev, "Resonant transparency and non-trivial non-radiating excitations in toroidal metamaterials," Sci. Rep. **3**(1), 2967 (2013).
84. A. A. Basharin, M. Kafesaki, E. N. Economou, C. M. Soukoulis, V. A. Fedotov, V. Savinov, and N. I. Zheludev, "Dielectric Metamaterials with Toroidal Dipolar Response," Phys. Rev. X **5**(1), 011036 (2015).
85. A. E. Miroshnichenko, A. B. Evlyukhin, Y. F. Yu, R. M. Bakker, A. Chipouline, A. I. Kuznetsov, B. Luk'yanchuk, B. N. Chichkov, and Y. S. Kivshar, "Nonradiating anapole modes in dielectric nanoparticles," Nat. Commun. **6**(1), 8069 (2015).
86. B. Ögüt, N. Talebi, R. Vogelgesang, W. Sigle, and P. A. van Aken, "Toroidal plasmonic eigenmodes in oligomer nanocavities for the visible," Nano Lett. **12**(10), 5239–5244 (2012).
87. J. Li, N. Verellen, and P. Van Dorpe, "Enhancing magnetic dipole emission by a nano-doughnut-shaped silicon disk," ACS Photonics **4**(8), 1893–1898 (2017).
88. Y. Yang, V. A. Zenin, and S. I. Bozhevolnyi, "Anapole-Assisted Strong Field Enhancement in Individual All-Dielectric Nanostructures," ACS Photonics **5**(5), 1960–1966 (2018).
89. E. M. Purcell, H. C. Torrey, and R. V. Pound, "Resonance absorption by nuclear magnetic moments in a solid," Phys. Rev. **69**(1–2), 37–38 (1946).
90. T. Taminiau, F. Stefani, F. B. Segerink, and N. Van Hulst, "Optical antennas direct single-molecule emission," Nat. Photonics **2**(4), 234–237 (2008).
91. S.-D. Liu, Z.-X. Wang, W.-J. Wang, J.-D. Chen, and Z.-H. Chen, "High Q-factor with the excitation of anapole modes in dielectric split nanodisk arrays," Opt. Express **25**(19), 22375–22387 (2017).
92. G. Grinblat, Y. Li, M. P. Nielsen, R. F. Oulton, and S. A. Maier, "Enhanced third harmonic generation in single germanium nanodisks excited at the anapole mode," Nano Lett. **16**(7), 4635–4640 (2016).
93. S.-D. Liu, J.-L. Fan, W.-J. Wang, J.-D. Chen, and Z.-H. Chen, "Resonance Coupling between Molecular Excitons and Nonradiating Anapole Modes in Silicon Nanodisk-J-Aggregate Heterostructures," ACS Photonics **5**(4), 1628–1639 (2018).
94. B. Luk'yanchuk, R. Paniagua-Domínguez, A. I. Kuznetsov, A. E. Miroshnichenko, and Y. S. Kivshar, "Hybrid anapole modes of high-index dielectric nanoparticles," Phys. Rev. A (Coll. Park) **95**(6), 063820 (2017).
95. D. E. Aspnes and A. Studna, "Dielectric functions and optical parameters of si, ge, gap, gaas, gasb, inp, inas, and insb from 1.5 to 6.0 ev," Phys. Rev. B Condens. Matter **27**(2), 985–1009 (1983).
96. P. B. Johnson and R.-W. Christy, "Optical constants of the noble metals," Phys. Rev. B **6**(12), 4370–4379 (1972).
97. Z. Huang, J. Wang, Z. Liu, G. Xu, Y. Fan, H. Zhong, B. Cao, C. Wang, and K. Xu, "Strong-field-enhanced spectroscopy in silicon nanoparticle electric and magnetic dipole resonance near a metal surface," J. Phys. Chem. C **119**(50), 28127–28135 (2015).
98. Y. Yang, O. D. Miller, T. Christensen, J. D. Joannopoulos, and M. Soljačić, "Low-loss plasmonic dielectric nanoresonators," Nano Lett. **17**(5), 3238–3245 (2017).
99. M. Khorasaninejad, J. Walia, and S. S. Saini, "Enhanced first-order Raman scattering from arrays of vertical silicon nanowires," Nanotechnology **23**(27), 275706 (2012).
100. M. O. Ali, N. Tait, and S. Gupta, "High-Q all-dielectric thermal emitters for mid-infrared gas-sensing applications," J. Opt. Soc. Am. A **35**(1), 119–124 (2018).
101. M. Robinson and J. Clegg, "Improved determination of Q-factor and resonant frequency by a quadratic curve-fitting method," IEEE T. Electromagn. C. **47**(2), 399–402 (2005).
102. N. Ganesh, I. D. Block, P. C. Mathias, W. Zhang, E. Chow, V. Malyarchuk, and B. T. Cunningham, "Leaky-mode assisted fluorescence extraction: application to fluorescence enhancement biosensors," Opt. Express **16**(26), 21626–21640 (2008).
103. L. Novotny and B. Hecht, *Principles of nano-optics* (Cambridge university, 2012).
104. E. L. Moal, E. Fort, S. Lévêque-Fort, F. P. Cordelières, M.-P. Fontaine-Aupart, and C. Ricolleau, "Enhanced fluorescence cell imaging with metal-coated slides," Biophys. J. **92**(6), 2150–2161 (2007).
105. M. J. Levene, J. Korlach, S. W. Turner, M. Foquet, H. G. Craighead, and W. W. Webb, "Zero-mode waveguides for single-molecule analysis at high concentrations," Science **299**(5607), 682–686 (2003).
106. J. Eid, A. Fehr, J. Gray, K. Luong, J. Lyle, G. Otto, P. Peluso, D. Rank, P. Baybayan, B. Bettman, A. Bibillo, K. Bjornson, B. Chaudhuri, F. Christians, R. Cicero, S. Clark, R. Dalal, A. Dewinter, J. Dixon, M. Foquet, A. Gaertner, P. Hardenbol, C. Heiner, K. Hester, D. Holden, G. Kearns, X. Kong, R. Kuse, Y. Lacroix, S. Lin, P. Lundquist, C. Ma, P. Marks, M. Maxham, D. Murphy, I. Park, T. Pham, M. Phillips, J. Roy, R. Sebra, G. Shen, J. Sorenson, A. Tomaney, K. Travers, M. Trulson, J. Vieceli, J. Wegener, D. Wu, A. Yang, D. Zaccarin, P. Zhao, F. Zhong, J. Korlach, and S. Turner, "Real-time DNA sequencing from single polymerase molecules," Science **323**(5910), 133–138 (2009).
107. C. I. Richards, K. Luong, R. Srinivasan, S. W. Turner, D. A. Dougherty, J. Korlach, and H. A. Lester, "Live-cell imaging of single receptor composition using zero-mode waveguide nanostructures," Nano Lett. **12**(7), 3690–3694 (2012).
108. J. Wenger, P.-F. Lenne, E. Popov, H. Rigneault, J. Dintinger, and T. Ebbesen, "Single molecule fluorescence in rectangular nano-apertures," Opt. Express **13**(18), 7035–7044 (2005).
109. L. P. Zaino 3rd, D. A. Grismer, D. Han, G. M. Crouch, and P. W. Bohn, "Single occupancy spectroelectrochemistry of freely diffusing flavin mononucleotide in zero-dimensional nanophotonic structures," Faraday Discuss. **184**, 101–115 (2015).

Optics EXPRESS

110. D. Punj, P. Ghenuche, S. B. Moparthi, J. de Torres, V. Grigoriev, H. Rigneault, and J. Wenger, "Plasmonic antennas and zero-mode waveguides to enhance single molecule fluorescence detection and fluorescence correlation spectroscopy toward physiological concentrations," Wiley Interdiscip. Rev. Nanomed. Nanobiotechnol. **6**(3), 268–282 (2014).
111. P. Ponzellini, X. Zambrana-Puyalto, N. Maccaferri, L. Lanzanò, F. De Angelis, and D. Garoli, "Plasmonic zero mode waveguide for highly confined and enhanced fluorescence emission," Nanoscale **10**(36), 17362–17369 (2018).

130.126.255.21 {ts '2019-02-27 13:57:57'}